Available online at www.sciencedirect.com
ScienceDirect
Journal of Magnetic Resonance 182 (2006) 283–292
JMR Journal of Magnetic Resonance
www.elsevier.com/locate/jmr

T_1 Measurements incorporating flip angle calibration and correction in vivo

Jinghua Wang [a,*], Maolin Qiu [a], Hyeonjin Kim [a], R. Todd Constable [a,b,c]

[a] Department of Diagnostic Radiology, Yale University School Medical Center, The Anlyan Center, 330 Cedar Street, P.O. Box 208042, New Haven, CT 06520-8042, USA
[b] Department of Biomedical Engineering, Yale University, New Haven, CT, USA
[c] Department of Neurosurgery, Yale University School of Medicine, New Haven, CT, USA

Received 1 November 2005; revised 27 June 2006
Available online 27 July 2006

Abstract

In this work, we propose a variable FA method that combines *in vivo* flip angle (FA) calibration and correction with a short TR variable FA approach for a fast and accurate T_1 mapping. The precision T_1s measured across a uniform milk phantom is estimated to be 2.65% using the conventional (slow) inversion recovery (IR) method and 28.5% for the variable FA method without FA correction, and 2.2% when FA correction is included. These results demonstrate that the sensitivity of the variable FA method to RF nonuniformities can be dramatically reduced when these nonuniformities are directly measured and corrected. The acquisition time for this approach decreases to 10 min from 85 min for the conventional IR method. In addition, we report that the averaged T_1s measured from five normal subjects are 900 ± 3 ms, 1337 ± 8 ms and 2180 ± 25 ms in white matter (WM), gray matter (GM) and cerebral spinal fluid (CSF) using the variable flip angle method with FA correction at 3 T, respectively. These results are consistent with previously reported values obtained with much longer acquisition times. The method reduces the total scan time for whole brain T_1 mapping, including FA measurement and calibration, to approximately 6 min. The novelty of this method lies in the *in vivo* calibration and the correction of the FAs, thereby allowing a rapid and accurate T_1 mapping at high field for many applications.

Keywords: RF inhomogeneity; RF calibration; Spin–lattice relaxation time; SSGE

1. Introduction

The spin–lattice relaxation time, T_1, varies between different tissues and pathologies, and therefore has been exploited as a contrast mechanism in MR imaging [1]. There has been strong interest in rapid and accurate T_1 measurements, which are essential for many research and clinic applications [2–4], such as spin labeling techniques [5] and dynamic contrast agent studies [6]. Conventionally, T_1 can be estimated using saturation-recovery (SR) sequences with multiple repetition times (TRs), or using inversion recovery (IR) sequences with multiple inversion times (TIs). However, these conventional sequences require long acquisition times in order to measure the longitudinal magnetization at the multiple time points needed for accurate T_1 measurements (typically with a resolution of 256×256, and 4–8 sampling points). To accelerate data acquisition, several approaches have been proposed. Look and Locker used a series of limited FA pulses to sample the T_1 recovery curve following a single inversion pulse [7]. Fast low angle shot (FLASH) sequences have also been employed with very short TR to rapidly acquire images for T_1 mapping [8,9]. However, these methods suffer from poor SNR due to the use of small flip angles. Although echo planar imaging (EPI) allows extremely fast image acquisitions with high SNR [10,11], the low spatial resolution and high sensitivity to magnetic field inhomogeneities limit its applicability. To overcome these shortages, a

* Corresponding author. Fax: +1 203 785 6534.
E-mail address: Jinghua.wang@yale.edu (J. Wang).

1090-7807/$ - see front matter © 2006 Elsevier Inc. All rights reserved.
doi:10.1016/j.jmr.2006.07.005

variable FA method, originally introduced in 1974 [12] and investigated by a number of authors [13–15], is used to estimate T_1 with an accuracy and a precision similar to that achieved by the IR and SR techniques, but with a significant reduction in acquisition time. However, since FAs vary spatially across an image due to RF/tissue interactions and/or from nonideal slice profiles, these variations in the FAs lead to errors in the measured T_1, particularly with the variable FA method. With a variable FA method, Luzikov et al. reported 15% errors in T_1 measurements with 10% errors in FAs [16,17], and Clare et al. [18] found 20% deviations in T_1 in a uniform phantom at 3 T. Therefore, it is critical to compensate imperfections in FA distribution when the variable FA method is used at high field (>1.5 T) [19].

In this work, we present a method for rapid and accurate T_1 mapping. Absolute FAs are obtained for each voxel through *in vivo* measurement of relative FAs and an FA calibration factor. Phantom and *in vivo* studies indicate that the precision and the accuracy of the T_1s measured by this method are comparable to those estimated using conventional IR-gradient echo (GE) sequences requiring much longer acquisition times.

2. Theory

2.1. Measurement of FA in vivo

For GE sequences, if TR is much longer than T_1 ($TR > 5T_1$) and T_2 ($TR > 5T_2$) of a sample, the signal intensity $SI(x)$ is given by [16,20,21],

$$\mathrm{SI}(x) = C(x) \cdot S(x) \cdot \sin\alpha(x), \tag{1}$$

where $\alpha(x)$, $\mathrm{SI}(x)$ and $S(x)$ are the excitation FA, the signal intensity, and the reception sensitivity at the position x in an image, respectively. The variable, $C(x)$, is dependent upon tissue properties (proton density, and T_2^*) and image acquisition parameters, such as echo time (TE) and TR. The ratio of signal intensities $\mathrm{SI}_{\alpha_1}(x)/\mathrm{SI}_{\alpha_2}(x)$of the two GE images at different nominal FAs α_1 and α_2 is given by

$$\lambda(x) = \frac{\mathrm{SI}_{\alpha_2}(x)}{\mathrm{SI}_{\alpha_1}(x)} = \sin\alpha_2(x)/\sin\alpha_1(x). \tag{2}$$

Note that Eq. (2) also assumes that the slice excitation profile for α_1 is identical to that for α_2. Based on this assumption, it is theoretically possible to estimate the actual value corresponding to α_1 at each voxel in a sample (denoted $\alpha_{1,\mathrm{meas}}(x)$) as previously described [16]. That is,

$$\alpha_{1,\mathrm{meas}}(x) = \arccos(\lambda(x)/2), \tag{3}$$

where $\alpha_2 = 2\alpha_1$ is assumed. Once this calibration process has been accomplished, the actual FA across the sample can be determined for any subsequent experiment (denoted $\alpha_{\mathrm{absolute}}(x)$) for which a nominal FA α_{nom} is specified. This is given by:

$$\alpha_{\mathrm{absolute}}(x) = k \cdot (\alpha_{1,\mathrm{meas}}(x)/\alpha_1) \cdot \alpha_{\mathrm{nom}}, \tag{4}$$

where k is a sample-specific FA calibration factor relating the input RF power to the actual FAs achieved. It is strongly dependent upon the electromagnetic properties of the sample and the relative position between the coil and the sample. The k factor is crucial to obtain absolute FA values as FA mapping generally only provides relative FA maps without calibration. The nominal FA is chiefly determined by the amplitude and duration of the applied RF pulse, however, the coupling between the RF coil and the sample can alter the flip angle achieved. Consequently, it is necessary to recalibrate the RF transmitter for each image acquisition *in vivo* if quantitative data are to be obtained. It is noted that the α_1 in Eq. (2) is the nominal FA used for determining $\alpha_{\mathrm{meas}}(x)$ and the absolute FA ($\alpha_{\mathrm{absolute}}$) corresponding to a nominal FA, α_{nom}, is calculated based on a linear relationship between the measured FA and the nominal FA.

If the FAs across a sample are uniform, k can be estimated using a free-induction decay (FID) experiment with different FAs. The actual FA of 90° yields the maximum signal intensity and the actual FA of 180° produces the null signal intensity for an FID at a long TR [24]. RF nonuniformities, however, negatively impact the use of such standard 90° and 180° methods (which do not take spatial variations into account) for estimating k. Other methods have been reported to estimate k taking into account spatial variations in flip angle with the penalty of additional scan time [25,26]. Here, we propose a method in which k is determined by the slope of the measured FA versus the nominal FA curve. The measured FA at each voxel is then scaled accordingly.

2.2. Measurement of T_1 using variable FA with RF correction terms

When the transverse magnetization dephases between successive RF excitation pulses within a TR, the signal intensity for an ideal steady-state gradient-echo (SSGE) sequence with an excitation FA of α can be approximated as [22]:

$$\mathrm{SI}(\alpha(x)) = M_0(x) \cdot \sin\alpha(x) \cdot \frac{(1 - E_1(x))}{1 - E_1(x) \cdot \cos\alpha(x)} \cdot S(x), \tag{5}$$

where $E_1(x) = \exp(-\mathrm{TR}/T_1(x))$. $M_0(\mathrm{x})$ and $S(x)$ are the equilibrium longitudinal magnetization and the receive sensitivity at the location x, respectively. In practice, the RF coil configuration, the interaction between a coil and a subject, and an imperfect slice profile produces variable FAs, such that the actual FA, $\alpha_{\mathrm{absolute}}(x)$, is a function of spatial location. Thus, Eq. (5) must be modified as [23]:

$$\frac{\mathrm{SI}_{\mathrm{measured}}(x)}{\sin(\alpha_{\mathrm{absolute}}(x))} = \frac{\mathrm{SI}_{\mathrm{measured}}(x)}{\tan(\alpha_{\mathrm{absolute}}(x))} \cdot E_1(x) + M_0(x) \cdot S(x) \cdot (1 - E_1(x)), \tag{6}$$

Finally, T_1 can be expressed as [15]:

$$T_1(x) = -\mathrm{TR}/\ln(E_1(x)). \tag{7}$$

Since the slope, E_1, depends only on a known TR and the unknown T_1, the T_1 will be independent of proton density, reception sensitivity, and T_2^*. Thus, the T_1 is calculated from the expression: $SI_{measured}(x)/\sin\alpha_{absolute}(x)$ vs. $SI_{measured}(x)/\tan\alpha_{absolute}(x)$.

2.3. Optimizing the T_1 acquisition

Many authors have investigated the optimum parameters for measuring T_1 at a fixed TR with a variable FA method [2,13,15]. For quantitative comparisons, we define a normalized dynamic range (DR) of regression as:

$$DR \propto \frac{1}{1 - E_1 \cos(\alpha_{1,nom})} - \frac{1}{1 - E_1 \cos(\alpha_{2,nom})}, \quad (8)$$

where $\alpha_{1,nom}$ and $\alpha_{2,nom}$ are the two nominal FAs used to estimate T_1. Using Eq. (8), we can numerically calculate the DR at different FAs in the two FAs and the results are shown in Fig. 1 for a T_1 of 1100 ms (the average T_1 of GM and WM at 3 T) and a TR of 500 ms. Evaluation of the DR and SNR over all possible combinations of FAs yields optimal FAs of 23° and 122° to minimize the error of T_1 measurement. This example also illustrates that the optimal FAs for T_1 measurements are a function of both the tissue T_1 and the TR.

2.4. Quantification of the linear relationship of the measured FA and nominal FA

To examine the range in which the linear relationship between the measured FA and the nominal FA holds, a normalized difference score parameter, ψ, can be defined as:

$$\psi(\alpha) = 2 * \frac{SI_{simulated}(\alpha) - SI_{measured}(\alpha)}{SI_{simulated}(\alpha) + SI_{measured}(\alpha)} * 100\%, \quad (9)$$

where $SI_{simulated}(\alpha)$ is the signal intensity of the image simulated according to Eq. (1) at the FA of α. The α is determined by the measured FA map using Eq. (4), based on the linear relationship. $SI_{measured}(\alpha)$ represents the signal intensity of the measured image at the FA of α. Small $\psi(\alpha)$ indicates that there is a good agreement between the measured FA and the nominal FA.

3. Methods

Five normal male adults with no history or physical findings of neurological diseases were studied. The mean age of the subjects was 37, (range from 25 to 45). The human study protocol was approved by the Institutional Review Board (IRB) at Yale University School of Medicine.

All phantoms and human brain images were acquired on a Siemens 3 T Trio system. Two cylindrical phantoms (15 cm in diameter) were used to evaluate the performance of the variable flip angle method with FA correction. One phantom was filled with 1% low fat milk (Deerfield farms) and the other was filled with oil. To examine the linear relationship between measured FAs and nominal FAs, measured FAs were obtained from both phantoms using a gradient echo sequence with α_1s varying from 20° to 180° in increments of 10°, and α_2 varying from 40° to 360° with increments of 20°. The signal intensity of the images with different FAs was simulated according to Eq. (1), assuming that $C(x)$ was constant for the homogeneous phantoms. $S(x)$ was calculated according to ref [20]. The actual FA map for each nominal FA was estimated from Eq. (4), based on the relative FAs and k which were calculated using the images acquired at the FAs of 30, 60, and 120°.

A conventional IR gradient echo pulse sequence (TI = 300, 600, 1000, 1500, 2000 ms) with nonslice selective

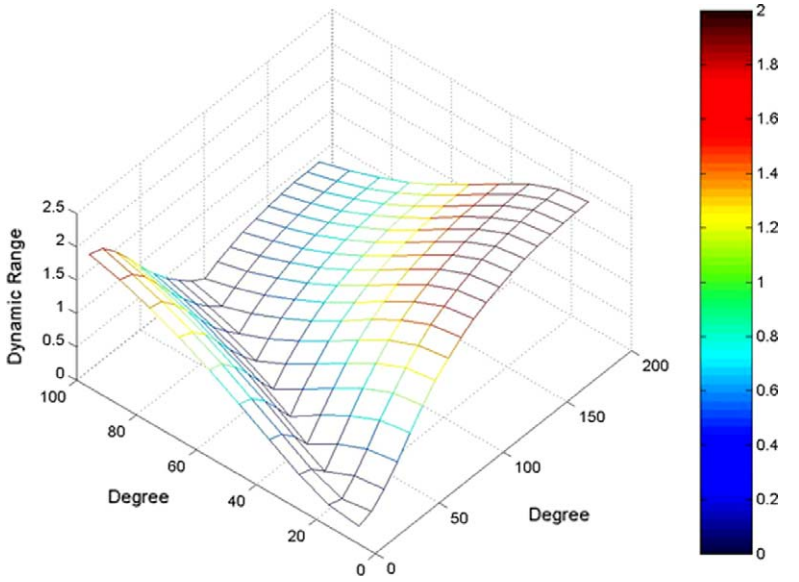

Fig. 1. The dynamic range DR as a function of the prescribed flip angle α_1 and α_2 at a TR = 500 ms with T_1 = 1100 ms. The optimum flip angles for minimizing the standard deviation of the T_1 are 23° and 122°.

IR magnetization preparation was used for T_1 mapping of the milk phantom and this T_1 was used as a reference. The total acquisition time was approximately 85 min. The measured FA map of the milk phantom was obtained using a segmented-EPI sequence with excitation FAs of 30°, 60°, and 120°, respectively. The EPI segmentation factor was 7. Other acquisition parameters for the gradient echo IR method were TR/TE 8000/4 ms, FOV 200×200 mm^2, matrix 128×128, and slice thickness of 5 mm. The T_1s of the phantom were estimated using a nonlinear three-parameter fitting from the images acquired with the IR gradient echo sequence at different TIs. For the variable FA method with FA correction, the two images were acquired using multi-slice gradient echo sequence at the FAs of 23° and 122°, TR/TE 150/4 ms. Other parameters were the same as those in the IR method.

The term "slice profile" refers to the magnitude component of transverse magnetization as a function of location along the slice select direction, which is typically a nonlinear profile of FAs described by the Bloch equations. The slice profile is closely related to RF pulses and the applied slice selection gradients. A spherical phantom (17 cm diameter) filled with distilled water and $NiSO_4{\cdot}H_2O$ (1.25 g/l), was used to quantitatively evaluate the effect of the RF pulse profile on the measured FA. Two multi-slice axial images were acquired from the spherical phantom using conventional gradient echo at FAs of 45° and 90° to evaluate the effect of RF pulse profile. These images were acquired with TR/TE 2500/4 ms, FOV 200×200 mm^2, matrix 128×128, slice thickness of 5 mm using three different RF excitation pulses (sinc, truncated sinc and Gaussian envelope profiles), with a 20 slice acquisition. The duration/bandwidth of the sinc, the truncated-sinc and the Gaussian RF pulses were 2.000/13.5, 5.120/20, and 5.120/10 ms/kHz, respectively. The measured relative FAs were calculated using Eq. (3) for these RF pulses. The calibration factor k for each RF pulse was determined from the slope of the measured FA vs. the nominal FA curves. After RF calibration, the absolute FA across the phantom was estimated according to Eq. (4). The T_1 map was then derived from Eqs. (6) and (7).

For the *in vivo* studies, the FA maps were acquired using a segmented spin echo EPI sequence with nominal excitation FAs of 30, 60 and 120°, with TR/TE of 2500/4 ms, FOV 240×192 mm^2, matrix 128×102, slice thickness of 6 mm, bandwidth 752 Hz per pixel, an EPI segment factor of 7, and a total acquisition time of 37 seconds for each acquisition. The effect of using a TR that did not satisfy the condition TR $\gg T_1$, was also examined with a TR of 1740 ms which was only about 1.5 times the average T_1 of GM and WM at 3.0 T. Since the measured FA map obtained at TR = 1740 ms did not significantly differ from that obtained at TR = 9000 ms [20], we concluded that the TR of 1740 ms could be used for FA mapping in GM and WM. The calibration of the FAs for human subjects was made assuming a linear relationship between the measured and nominal FAs. An *in vivo* calibration factor was calculated from the slope of the plot of the measured FA versus the nominal FA (measured from the 30°/60° acquisitions) for each subject. Finally, T_1 maps were estimated using the two gradient echo images with the nominal FAs of 23 and 122°, and short TR. Other acquisition parameters were: FOV 240×192 mm^2, matrix 256×204, slice thickness 3 mm, TR/TE 500/4 ms, 40 slices, and a bandwidth of 360 Hz per pixel. The *in vivo* images were processed with the following steps: (1) low-intensity background noise, skull and extra-cranial tissues were all set to zero; (2) the images obtained in different acquisitions were registered to reduce the influence of mis-registration/motion on the measured T_1 [27]; (3) the T_1 of each voxel was estimated. Since the T_1 of each brain tissue is usually not reflected by a single value but by a distribution of values [28], histograms of the measured T_1s were fit using three Gaussian distributions representing the three main tissues: CSF, GM, and WM. The T_1 of each tissue is then expressed as the mean of its Gaussian distribution.

4. Results

The measured versus the nominal FAs curves for the oil and milk phantoms are shown in Fig. 2a and b, respectively. The standard deviation (SD) of the measured FA is estimated for the whole FOV. The result shows that the linear relationship holds for both phantoms when the measured FA is less than 120°. Since the measured FA at 120° is actually calculated from images obtained at nominal FAs of $\alpha_1 = 120°$and $\alpha_2 = 240°$, this result indicates that the apparent nonlinearity of the measured FA above 120° is due to the nonlinearity of α_2 when α_2 is greater than 240°. The measured FAs in the milk phantom show greater nonuniformities compared to those measured with the oil phantom, as indicated by the larger error bars particularly at higher FAs.

The simulated images with actual FAs and receive sensitivity are shown in Fig. 3a for the oil phantom, and Fig. 3c for the phantom containing milk. The corresponding, experimentally measured images are displayed in Fig. 3b (oil), and Fig. 3d (milk). For the oil phantom, the simulated image is similar to the measured image even at the nominal FA of 240°, suggesting the linear relationship holds over this range. For the milk phantom, however, the image is significantly different from the measured image at that nominal FA.

Fig. 4 shows the normalized difference score, ψ, between the simulated and the measured images for the oil and milk phantoms shown in Fig. 3. In Fig. 4a (oil), ψ is less than 5%, and the simulated images are in good agreement with the measured images. In Fig. 4b (milk) the images are also in good agreement except over the range of $160° < \alpha < 240°$, where ψ is more than 5%. The discrepancy is primarily due to the low SNR in this FA range. Here the ψ value of 5% reflects a "transition point" from linear to nonlinear behavior.

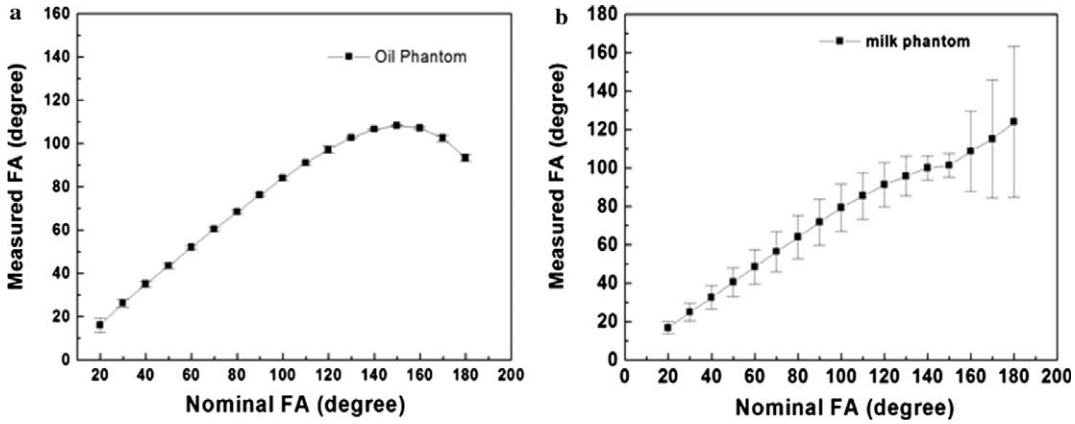

Fig. 2. Plots showing the linear relationship between the measured flip angle and the prescribed nominal flip angle for phantoms containing oil (a) and milk (b).

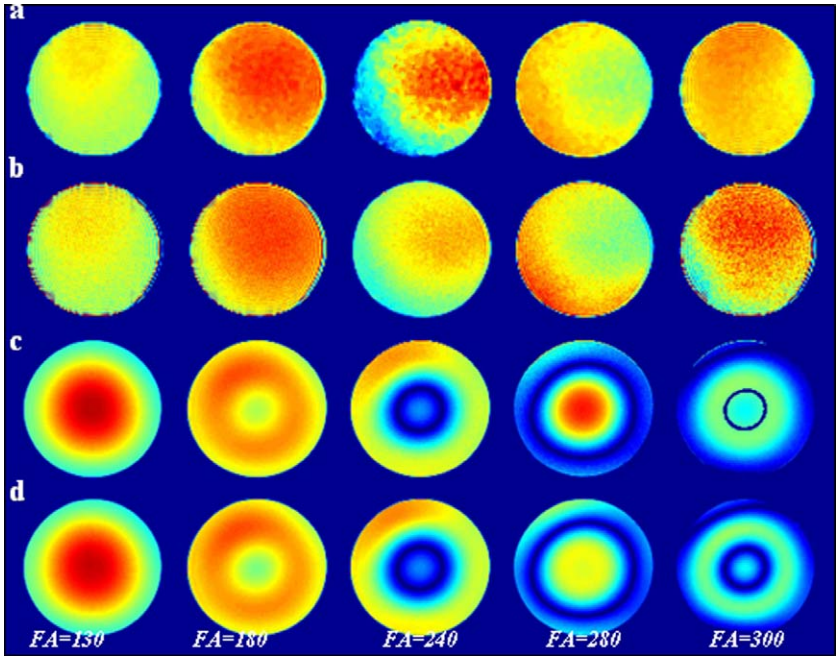

Fig. 3. Simulated images rows (a and c), assuming a linear relationship between the prescribed flip angle and the nominal flip angle, and the measured images, rows (b and d), for the phantom containing oil (a and b) and milk (c and d) at different flip angles.

Moreover, FA calibration factors, *k*s, in Eq. (4) are easily estimated from the slopes of the averaged measured FA vs. the nominal FA curves of the phantoms shown in Fig. 2a and b, respectively. The slopes are 0.82 and 0.78 for the oil and milk phantoms, respectively, at nominal FAs lower than 120°. The normalized difference scores also support this calculation. For the oil phantom, the maximum peak in the difference score shown in Fig. 4a occurs at a FA of ~220°, which is in contrast to the theoretically predicted value of 180° ; the standard nulling point. The ratio, 180/220°, is 0.82 which is identical to the slope calculated from Fig. 2. For the milk phantom, the FA exhibits sufficient RF inhomogeneity from the RF wave behavior such that the normalized difference score cannot provide this ratio. The difference in the *k* factors between the milk and oil phantoms emphasizes that *k* must be estimated for each sample, because the RF field response is sample dependent.

Fig. 5 displays the measured FA maps for (a) Gaussian, (b) sinc, and (c) truncated-sinc, RF pulses. The magnitude of the measured FA is normalized to a nominal FA of 45°. For each of these RF pulses, the largest FA (or strongest RF field) occurs at the center of the phantom in Fig. 5. The FA is largest for the sinc RF pulse, and smallest for the Gaussian RF pulse. The maximum differences in the measured FA maps between these pulses are larger than the standard deviation of the measured FA (which is approximately 2%), suggesting that RF pulse profiles influence the measured FA maps and subsequent T_1 measurements. Even for RF pulses in the same category (sinc and

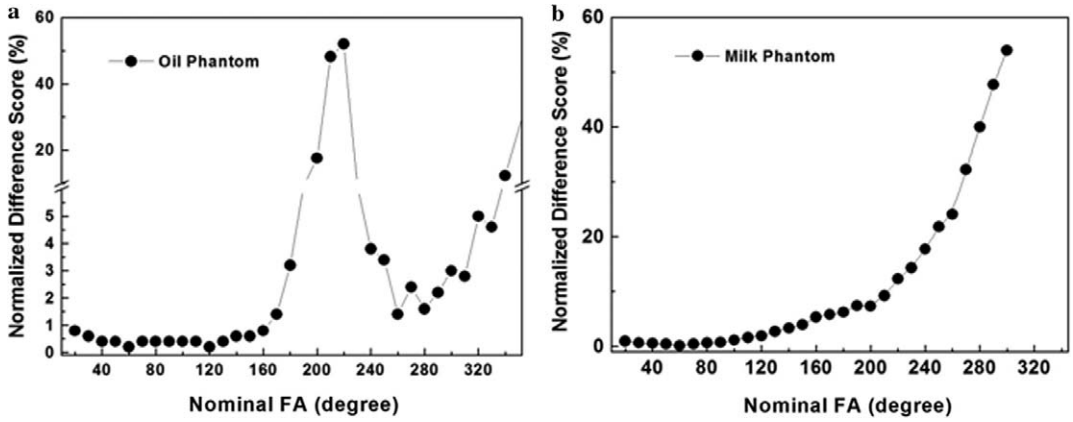

Fig. 4. The normalized difference score between the simulated images and the measured images for different flip angles for the phantom containing oil (a) and milk (b).

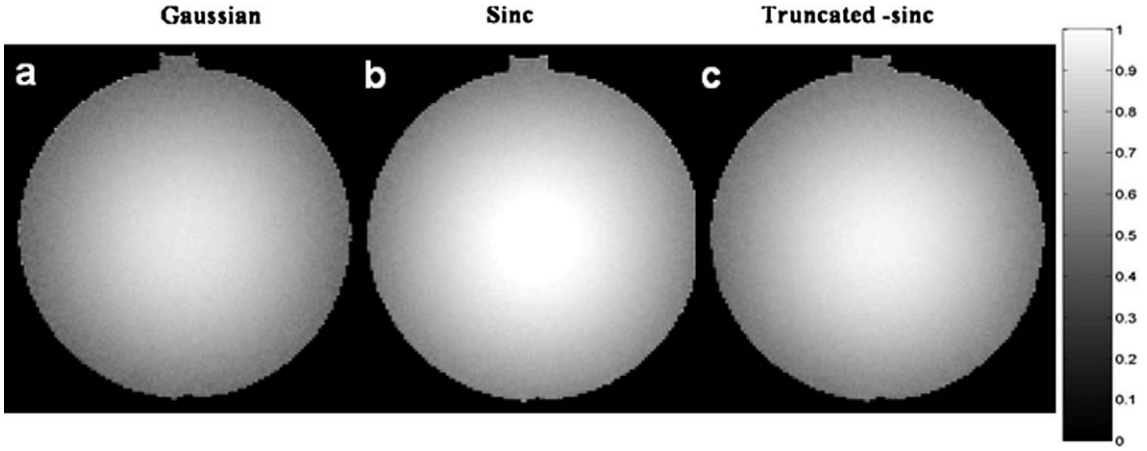

Fig. 5. The measured flip angle map for different RF pulses: Gaussian (a), sinc (b), and truncated sinc (c) at a nominal flip angle of 60°.

truncated-sinc), the truncated pulse design leads to a different pulse profile, which in turn leads to a different distribution of the measured FA map as shown in Fig. 5b and c. The results demonstrate that the variable flip angle approach with FA correction is sensitive to the slice profile, and that the influence of the slice profile on the measured T_1 is accounted for with the FA mapping and calibration.

Fig. 6a shows the measured FA map of a milk phantom using a segmented-EPI sequence at the nominal FAs of 30°, 60°, and 120°. The measured FA map, calculated according to Eq. (4), demonstrates significant nonuniformities. The standard deviation of the measured FA over the entire phantom is 19% of the mean. The T_1 images of the phantom, estimated from the two acquisitions at FAs of 23° and 122°, with the variable flip angle method with, and without FA correction, are shown in Fig. 6b and c, respectively. With the variable FA method, the T_1 is 1190 ± 340 ms, with the standard deviation approximately 28.5% of the mean T_1. With flip angle correction, the average T_1 is 1493 ± 33 ms, with the standard deviation reduced to only 2.2% of the mean. Using a gradient echo IR method with different TIs and an overall acquisition time of approximately 85 min, the T_1 image calculated with a three parameter nonlinear fitting routine is shown in Fig. 6d. The T_1 is 1391 ± 37 ms with the standard deviation representing only 2.6% of the mean.

The average k of the five subjects is 0.74, suggesting that a measured FA is generally smaller than the nominal FA *in vivo*. A representative FA map is shown in the top row of Fig. 7. In the FA map, the standard deviation across the slice is approximately 20% of the mean measured FA. With the variable FA method, the error in the measured FA propagates to the measured T_1. Thus, the T_1 of GM in certain regions is comparable to that of the WM, as shown in the middle row of Fig. 7. Using the variable flip angle approach with FA correction, the error in the measured T_1 is significantly reduced to around 2%. Thus, the T_1 of GM and WM exhibits excellent contrast, as shown in Fig. 7 (bottom row). Across the 5 subjects, the average T_1s is: 900 ± 3 ms for WM, 1337 ± 8 ms for GM and 2180 ± 25 ms for CSF.

5. Discussion

As field strength increases, T_1 becomes longer and the constraint, $TR > 5T_1$, for conventional T_1 mapping leads

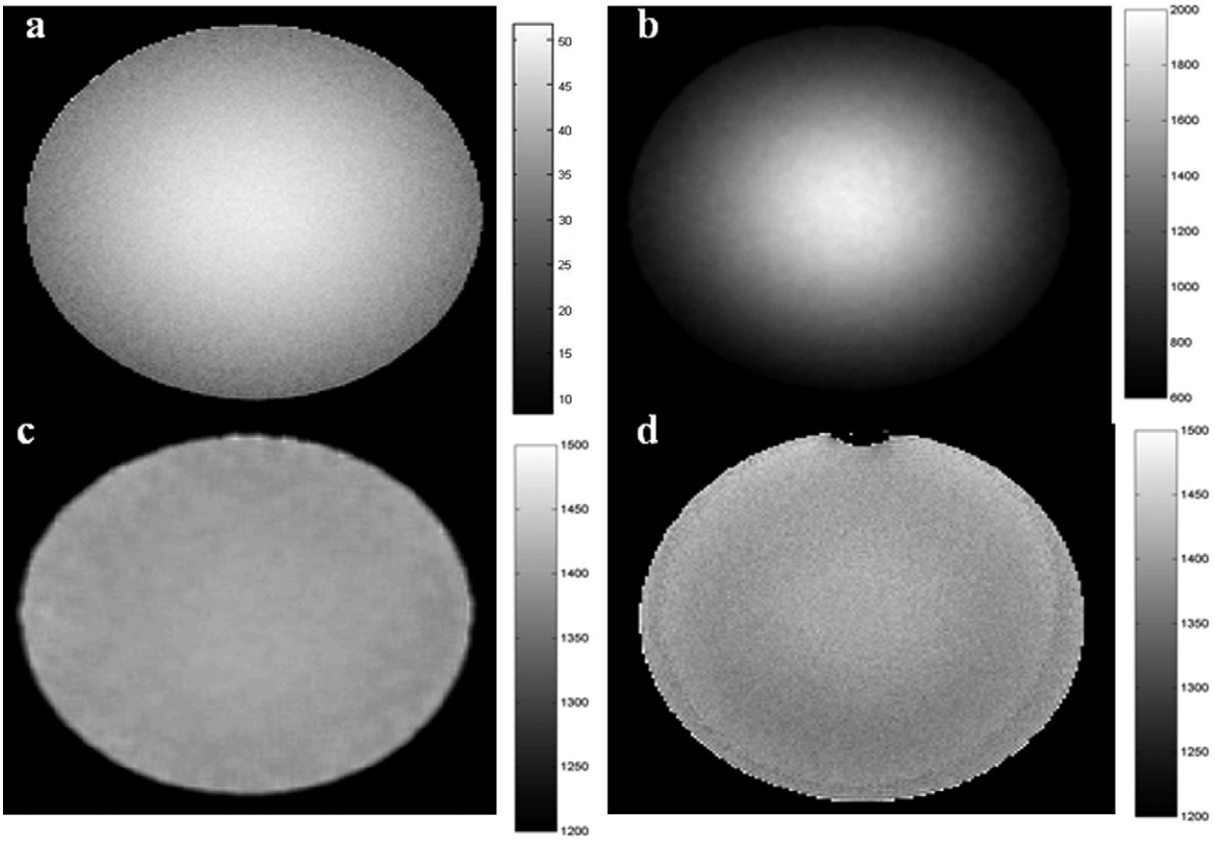

Fig. 6. A flip angle map (a) at a nominal flip angle of 45°, and the corresponding T_1 map before (b) and after (c) correction of RF non-uniformity based on the flip angle map for the phantom containing milk with the variable FA method, and the T1 map measured by conventional inversion recovery (d).

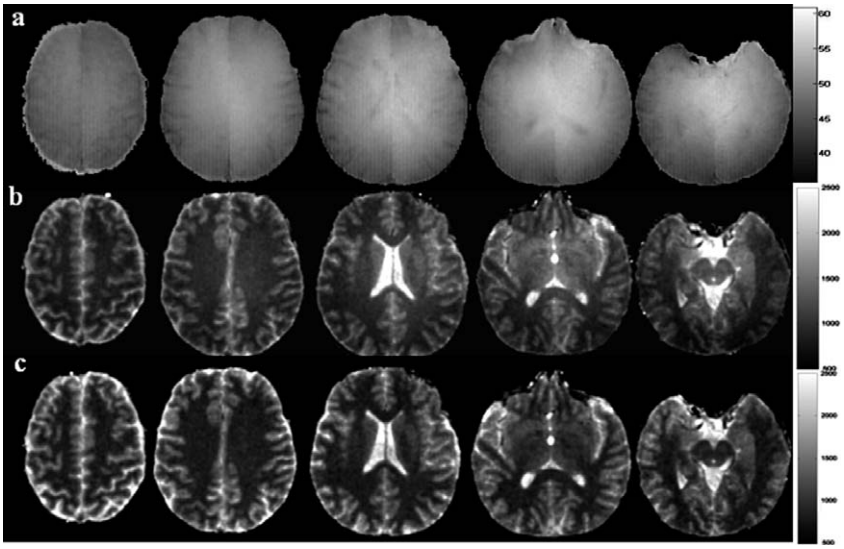

Fig. 7. The *in vivo* measured FA map (row a), and T_1 maps obtained using the variable flip angle approach before (row b), and after (row c), *in vivo* flip angle mapping, calibration, and correction of the flip angle non-uniformity.

to prohibitively long acquisition times. Short TR gradient echo imaging with a variable FA method provides a means for rapid T_1 mapping but is highly sensitive to RF inhomogeneity. Ropele et al. [29], previously showed that large errors in T_1 mapping arose from variations in the measured FA caused by RF inhomogeneities or by nonideal slice profiles. By implementing the variable FA method, Wang et al. found a 10% standard deviation for $T_1 = 1000$ ms at 1.5 T [13]. Mintzopoulos et al. [30], showed that errors in T_1 of as much as 17% were obtained at 3 T, and the data presented above showed a 29% standard deviation for a phantom containing milk (Fig. 6b). These results demonstrate that

with the variable FA method RF nonuniformities lead to significant errors in the measured T_1. Thus, it is necessary to correct for these effects. Venkatesan et al. [24] proposed an RF correction scheme that was only valid at low field where the transmission field and the reception sensitivity may be assumed to be identical [31]. Parker et al. [32], proposed a method to correct the effect of RF inhomogeneities on the measured T_1 at 1.5 T. Both Venkatesan and Parker assumed that the transmission field and the reception sensitivity in a phantom were identical to those in a human brain at 1.5 T. However, neither of these assumptions is valid at high field. Our experimental results demonstrated that both the measured FA and the FA calibration factor were sample-dependent, and thus should be specifically measured for each sample. The strength of the variable flip angle approach with FA correction that we present here, is that the correction is tailored to the sample being imaged.

Generally, the relative FA map determines the precision or the error in the measured T_1. The accuracy of the measured T_1 is determined by the absolute FA, which includes both the relative FA and the FA calibration factor. There is no gold standard for validating *in vivo* human brain T_1 measurements. Such an evaluation is difficult due to many factors that can influence the T_1, such as temperature, partial volume effects, radiation damping, chemical exchange and perfusion. In this work, the T_1s reported by the other authors can be used to evaluate our proposed approach. Kim et al. [33], obtained a T_1 of 939 for WM and 1354 ms for GM at 4 T. Wansapura et al. [34] reported a T_1 of 832 ms for WM and 1331 for GM at 3 T. With our proposed approach, the average T_1 in five subjects was 900 ± 3 ms for WM, and 1337 ± 8 ms for GM. The T_1s for WM and GM were 7.5% and 0.4% higher, respectively, than those obtained with Wansapura's method. Such discrepancy might arise from the fact that their T_1 values were measured in a specific region of interest (ROI), while our T_1s were obtained from all of the tissue via fitting three Gaussian curves to the whole brain histogram. Partial volume effects could have affected the accuracy of the ROI method but should not influence the histogram fitting [28], possibly accounting for the difference in these values. With our proposed approach, the *in vivo* FA maps were measured at TR = 2500 ms which was shorter than T_1 of CSF at 3 T. Errors in the FA estimation for voxels including CSF may have led to an underestimation of the T_1 in CSF. Moreover, the FAs of 23 and 122° for estimating the T_1 *in vivo* were optimal only for GM and WM at 3 T. Thus, there was larger error in the measured T_1 of CSF.

Since scan time strongly influences the SNR of the images used for T_1 calculations, an efficiency term can be defined to assess the effect of SNR on T_1 as

$$\eta = \frac{T_1}{\sigma_{T_1} \cdot \sqrt{T_{\text{total}}}} \tag{10}$$

where σ_{T_1} is the standard deviation of a measured T_1, and T_{total} represents the total scan time for estimating the measured T_1. Crawley and Henkelman [35], showed maximum η could be achieved by sampling just five TI points along the recovery curve at $\text{TR} = 3T_1$ using an IR method, compared to the methods of snapshot flash, Look–Locker, and accelerated Look–Locker. In this work, the η of the optimal IR method, is compared with the variable FA method with and without RF correction. The acquisition time for FA mapping is also included in the total acquisition time for our approach.

At the same spatial resolution, the efficiency η, is improved from $0.14\ s^{1/2}$ with the variable FA method to $1.9\ s^{1/2}$ when RF correction is included, while an η of $0.52\ s^{1/2}$ is obtained with the optimized IR method. These results indicate that the variable flip angle approach is not only rapid, but also has high η for estimating T_1 mapping, compared to the other methods. It is also noted that the η for the variable FA approach without correction is lower than that of the optimized IR method at 3 T emphasizing the need for FA correction and calibration at high field strength.

The sources of error in the T_1 measurements obtained with our method arise from several factors including, thermal noise, misregistration either between the actual FA map and the T_1 acquisitions, or between different FA acquisitions alone, and off-resonance effects [36]. Tissue T_1 may also vary with RF pulse-induced temperature changes, and other factors such as blood flow, chemical exchange as well as magnetic susceptibility.

The approach presented here has several advantages and disadvantages over the conventional IR method in T_1 measurement, particularly at high field strength. (1) Human tissue T_1 increases with the increasing static magnetic field, thus requiring increased scan time for estimating T_1 with conventional IR method. For the variable flip angle approach incorporating RF correction, longer T_1s have little influence on the scan time. (2) The variable flip angle approach substantially shortens the scan time and thus is highly efficient with an approximately unchangeable precision. (3) The specific absorption rate (SAR) becomes a limiting factor for some sequences at high field and the elimination of multiple IR pulses can significantly reduce SAR. Decreasing SAR increases the temperature stability of the tissue being imaged, and reduces the effect of temperature on the measured T_1. (4) Our method may reduce the influence of chemical exchange on the measured T_1 due to a short TR [37]. (5) Without the need for IR pulses, our approach may reduce the effect of magnetization transfer on the measured T_1. (6) Different slice profiles for the nominal FAs of 23 and 122° have different influences on the measured T_1 without FA correction. Because FA maps are very sensitive to the slice profiles as shown in Fig. 5, the different slice profiles for the two FAs can give rise to the difference in FA maps. With RF correction, the error resulting from the different slice profiles is taken into account. Finally, though magnetization transfer effects have a small influence on the measured T_1, they do affect the accuracy of the measured T_1 for multi-slice imaging and this could be an issue of with the variable flip angle

method. Such effects can be reduced if a hard RF pulse is applied to estimate the T_1. In this work, the acquisition parameters for T_1 measurements were optimized only for GW and WM, and therefore, the measured T_1 of CSF was subject to greater error. It is difficult to optimize this approach for CSF as there can be larger errors in FA maps for the voxels including CSF because the TR used in FA mapping is typically short compared to the T_1 of CSF. These errors give rise to the underestimation of the CSF T_1.

6. Conclusions

In this work, we demonstrate that it is possible to achieve fast and accurate T_1 mapping with the variable flip angle method if FA calibration and correction is used. This approach strongly depends on a precise knowledge of the absolute FA for each voxel. This knowledge can be obtained by calculating relative FA maps and calibration factors *in vivo*. Experimental results indicate that FA mapping and calibration are sample-dependent, thus, the absolute FA must be measured *in vivo*. Compared with conventional IR methods, our approach demonstrates high efficiency in obtaining T_1 measurements. *In vivo* results reveal excellent T_1 images with a short total acquisition time, even taking into account the time required for *in vivo* RF calibration and field mapping. The novelty of this method lies in the *in vivo* calibration and correction of the FAs, thereby allowing rapid and accurate T_1 mapping at high field for many applications.

Acknowledgments

This work was partially supported by NS40497, NS38467, and EB00473.

References

[1] P.A. Bottomley, C.J. Hardy, R.E. Argersinger, G. Allen-Moore, A review of 1H nuclear magnetic resonance relaxation in pathology: are T1 and T2 diagnostic? Med. Phys. 14 (1987) 1–37.
[2] S.C. Deoni, B.K. Rutt, T.M. Peters, Rapid combined T1 and T2 mapping using gradient recalled acquisition in the steady state, Magn. Reson. Med. 49 (2003) 515–526.
[3] J. Vymazal, A. Righini, R.A. Brooks, M. Canesi, C. Mariani, M. Leonardi, G. Pezzoli, T1 and T2 in the brain of healthy subjects, patients with Parkinson's disease, and patients with multiple system atrophy: relation to iron content, Radiology 211 (1999) 489–495.
[4] L. Vaithianathar, C.R. Tench, P.S. Morgan, C.S. Constantinescu, Magnetic resonance imaging of the cervical spinal cord in multiple sclerosis–a quantitative T1 relaxation time mapping approach, J. Neurol. 250 (2003) 307–315.
[5] J.A. Detre, J.S. Leigh, D.S. Williams, A.P. Koretsky, Perfusion imaging, Magn. Reson. Med. 23 (1992) 37–45.
[6] J. Zheng, R. Venkatesan, E.M. Haacke, F.M. Cavagna, P.J. Finn, D. Li, Accuracy of T1 measurements at high temporal resolution: feasibility of dynamic measurement of blood T1 after contrast administration, J. Magn. Reson. Imaging 10 (1999) 576–581.
[7] D.C. Look, D.R. Locker, Time saving in measurement of NMR and EPR relaxation times, Rev. Sci. Instrum. 41 (1970) 250–251.
[8] A. Haase, Snapshot FLASH MRI. Application to T1, T2, and chemical-shift imaging, Magn. Reson. Med. 13 (1990) 77–89.
[9] R. Deichmann, D. Hahn, A. Haase, Fast T1 mapping on a whole-body scanner, Magn. Reson. Med. 42 (1999) 206–209.
[10] P. Gowland, P. Mansfield, Accurate measurement of T1 in vivo in less than 3 seconds using echo-planar imaging, Magn. Reson. Med. 30 (1993) 351–354.
[11] A.J. Freeman, P.A. Gowland, P. Mansfield, Optimization of the ultrafast Look–Locker echo-planar imaging T1 mapping sequence, Magn. Reson. Imaging 16 (1998) 765–772.
[12] K.A. Christensen, D.M. Grand, E.M. Schulman, C. Walling, Optimal determination of relaxation times of Fourier transform nuclear magnetic resonance. Determination of spin-lattice relaxation times in chemically polarized species, J. Phys. Chem. 78 (1974) 1971–1977.
[13] H.Z. Wang, S.J. Riederer, J.N. Lee, Optimizing the precision in T1 relaxation estimation using limited flip angles, Magn. Reson. Med. 5 (1987) 399–416.
[14] E.K. Fram, R.J. Herfkens, G.A. Johnson, G.H. Glover, J.P. Karis, A. Shimakawa, T.G. Perkins, N.J. Pelc, Rapid calculation of T1 using variable flip angle gradient refocused imaging, Magn. Reson. Imaging 5 (1987) 201–208.
[15] S.C. Deoni, T.M. Peters, B.K. Rutt, Determination of optimal angles for variable nutation proton magnetic spin–lattice, T1, and spin–spin, T2, relaxation times measurement, Magn. Reson. Med. 51 (2004) 194–199.
[16] R. Stollberger, P. Wach, Imaging of the active B1 field in vivo, Magn. Reson. Med. 35 (1996) 246–251.
[17] Y. Luzikov, N.M. Sergeyev, M.G. Levkovitch, The "rapid" modification of the progressive saturation technique, J. Magn. Reson. 21 (1976) 359–363.
[18] S. Clare, M. Alecci, P. Jezzard, Compensating for B(1) inhomogeneity using active transmit power modulation, Magn. Reson. Imaging 19 (2001) 1349–1352.
[19] I.R. Young, D.J. Bryant, J.A. Payne, Variations in slice shape and absorption as artifacts in the determination of tissue parameters in NMR imaging, Magn. Reson. Med. 2 (1985) 355–389.
[20] J. Wang, M. Qiu, Q.X. Yang, M.B. Smith, R.T. Constable, Measurement and correction of transmitter and receiver induced nonuniformities in vivo, Magn. Reson. Med. 53 (2005) 408–417.
[21] J. Wang, M. Qiu, R.T. Constable, A method for rapid and effective correction of signal intensity nonuniformities with phased array coils in vivo, Magn. Reson. Med. 53 (2005) 666–674.
[22] R.R. Ernst, W.A. Anderson, Applications of fourier transform spectroscopy to magnetic resonance, Rev. Sci. Instrum. 37 (1966) 93–102.
[23] R.K. Gupta, A new look at the method of variable nutation angle for the measurement of spin–lattice relaxation times using Fourier transform NMR, J. Magn. Reson. 25 (1977) 231–235.
[24] R. Venkatesan, W. Lin, E.M. Haacke, Accurate determination of spin-density and T1 in the presence of RF-field inhomogeneities and flip-angle miscalibration, Magn. Reson. Med. 40 (1998) 592–602.
[25] G.J. Barker, A. Simmons, S.R. Arridge, P.S. Tofts, A simple method for investigating the effects of non-uniformity of radiofrequency transmission and radiofrequency reception in MRI, Br. J. Radiol. 71 (1998) 59–67.
[26] D.L. Foxall, B.E. Hoppel, H. Hariharan, Calibration of the radio frequency field for magnetic resonance imaging, Magn. Reson. Med. 35 (1996) 229–236.
[27] D. Rueckert, L.I. Sonoda, C. Hayes, D.L. Hill, M.O. Leach, D.J. Hawkes, Non-rigid registration using free-form deformations: Application to breast MR images, IEEE Trans. Med. Imaging 18 (1999) 712–721.
[28] F.R. Fenrich, C. Beaulieu, P.S. Allen, Relaxation times and microstructures, NMR Biomed. 14 (2001) 133–139.
[29] S. Ropele, R. Stollberger, F. Ebner, F. Fazekas, T1 imaging using phase acquisition of composite echoes, Magn. Reson. Med. 41 (1999) 386–391.

[30] D. Mintzopoulos, S. Inati, Accurate high-resolution T1 mapping in vivo, Proc. Int. Soc. Magn. Reson. Med., Miami 13 (2005) 1242.
[31] G.H. Glover, C.E. Hayes, N.J. Helc, W.A. Edelstein, O.M. Mueller, H.R. Hart, C.J. Hardy, M.O. Donnell, W.D. Barber, Comparison of linear and circular polarization for magnetic resonance imaging, J. Magn. Reson. 64 (1985) 255–270.
[32] G.J. Parker, G.J. Barker, P.S. Tofts, Accurate multislice gradient echo T(1) measurement in the presence of non-ideal RF pulse shape and RF field nonuniformity, Magn. Reson. Med. 45 (2001) 838–845.
[33] S.G. Kim, X. Hu, K. Ugurbil, Accurate T1 determinations from inversion recovery images: application to human brain at 4 Tesla, Magn. Reson. Med. 31 (1994) 445–449.
[34] J.P. Wansapura, S.K. Holland, R.S. Dunn, W.S. Ball, NMR relaxation times in the human brain at 3.0 tesla, J. Magn. Reson. Imaging 9 (1999) 531–538.
[35] A.P. Crawley, R.M. Henkelman, A comparison of one shot and recovery methods in T1 imaging, Magn. Reson. Med. 7 (1988) 23–34.
[36] P.B. Kingsley, W.G. Monahan, Correcting for incomplete saturation and off-resonance effects in multiple-site saturation-transfer kinetic measurements, J. Magn. Reson. 146 (2000) 100–109.
[37] R.G. Spencer, K.W. Fishbein, Measurement of spin–lattice relaxation times and concentrations in systems with chemical exchange using the one-pulse sequence: breakdown of the Ernst model for partial saturation in nuclear magnetic resonance spectroscopy, J. Magn. Reson. 142 (2000) 120–135.